Letters on Materials 15 (4), 2025 pp. 270-276 www.lettersonmaterials.com

Received 15 September 2025; Accepted 14 October 2025
https://doi.org/10.48612/letters/2025-4-270-276
https://elibrary.ru/uuuloy

The effect of grain-boundary "shells" on the mechanical properties of an Al alloy

B. B. Straumal[†1], A. S. Gornakova[1], M. A. Khorosheva[1], N. N. Khrapova[1], G. S. Davdyan[1], V. I. Orlov[1], N. S. Afonikova[1], O. A. Kogtenkova[1], V. A. Avtonomov[2], A. N. Nekrasov[3], B. B. Eshov[4]

[†]straumal@issp.ac.ru

[1]Osipyan Institute of Solid State Physics, Russian Academy of Sciences, Chernogolovka 142432, Russia
[2]Cotton Breeding, Seed Production and Agrotechnologies Research Institute, Salar, Kibrai district, Tashkent vilajat 111218, Uzbekistan
[3]Korzhinskii Institute of experimental mineralogy, Russian Academy of Sciences, Chernogolovka 142432, Russia
[4]Center for Research of Innovative Technologies, National Academy of Sciences of Tajikistan, Dushanbe 734012, Tajikistan

Abstract: In this paper, the grain boundary (GB) wetting phase transition in aluminum-based 1163 alloy is studied. The transition from incomplete GB wetting to complete one occurs in the temperature range from 520 to 600°C. Below 520°C, the melt enriched in copper and magnesium forms separate lenticular droplets at the GBs. Above 520°C, the melt forms continuous layers along almost all boundaries between aluminum grains. In such a way, the melt forms a kind of liquid shell around each matrix grain. During quenching after annealing, the grain boundary "shells" solidify and consist mainly of the ternary intermetallic compound Al_2CuMg. Previously, we observed that such GB "shells" of the second phase can significantly change, for example, the electrical or magnetic properties of a polycrystal. In this paper, we found for the first time that a change in the fraction of completely wetted GBs can also affect the mechanical properties of the material after quenching. In particular, in samples annealed below 520°C, when there are no completely wetted GBs, the conditional yield strength $\sigma_{0.2}$ does not change. Above 520°C, as the fraction of completely wetted GBs increases, the $\sigma_{0.2}$ value rapidly decreases by about one and a half times to 600°C. At the same time, the Young's modulus, which is determined mainly by the bulk properties of aluminum grains, remains virtually unchanged with increasing temperature and increasing fraction of completely wetted GBs. Thus, the effect we have discovered provides materials scientists with a fundamentally new tool for purposeful modification of mechanical properties of various polycrystalline materials.

Keywords: grain boundaries, wetting, Al alloys, mechanical properties

Acknowledgements: *This work was supported by the Russian Ministry of Science and Higher Education (contract no. 075-15-2025-664 grant no. 13.2251.21.0314).*

1. Introduction

If a solid polycrystal S contains a small amount of the liquid phase L, then this second phase may be distributed differently along the boundaries between the matrix grains. Thus, if the energy of the two interphase boundaries $2\sigma_{SL}$ is higher than the energy σ_{GB} of the grain boundary (GB) in the matrix, $2\sigma_{SL} > \sigma_{GB}$, then the second phase in the GB has the shape of isolated, usually lenticular droplets or particles. These droplets form a non-zero contact angle θ with the GB. This case is called incomplete wetting of the GB by the second phase. If the energy of the two interphase boundaries is less than the GB energy, $2\sigma_{SL} < \sigma_{GB}$, then it is energetically advantageous for the system to replace the GB with a second phase interlayer. In this case, we are dealing with the complete GB wetting by the second phase. If all the GBs are completely wetted, then the second phase forms a set of thin layers in the polycrystal, which completely surround the matrix crystallites like shells and separate them from each other. In a number of cases, when external conditions (such as temperature [1, 2] or pressure [3]) change, a reversible phase transition occurs from incomplete GB wetting by the second phase to complete one and vice versa. Such a change in the topology of the spatial distribution of the second phase can significantly affect various properties of polycrystals. For example, in the Cu-Bi system, bismuth can form thin grain-boundary layers with low conductivity in a copper matrix with high conductivity [4]. If the bismuth layers surround all the copper grains, then the conductivity of such a sample is low. If, by changing the pre-annealing temperature, the network of grain boundary layers is gradually destroyed, then at some point percolation occurs in the polycrystal and a continuous path through the copper grains is formed, not broken by the bismuth interlayers, and the conductivity of the polycrystal increases sharply [4]. Similarly, the network of GB layers, the grain boundary "shells", is the reason for the appearance of ferromagnetic properties in zinc oxide [5–8]. Thin layers of the GB phase may also increase the GB diffusion permeability [9–12].

All these facts allow us to expect that changes in the morphology of the GB layers can significantly affect the mechanical properties of polycrystals. In order to test this hypothesis, we chose aluminum alloy 1163, in which (a) a reversible transition occurs from incomplete wetting of Al/Al grain boundaries by the melt, (b) below a certain temperature T_{wmin} the polycrystal does not contain completely wetted GBs (c) above a certain temperature T_{wmax}, all Al/Al GBs are completely wetted by the melt, (d) the temperature range between T_{wmin} and T_{wmax} is wide enough to accommodate several experimental points, (e) the selected aluminum alloy 1163 is widely used and its mechanical properties are not only of academic, but also of a practical interest.

2. Materials and methods

The 1163 aluminum alloy was chosen as the object of the study. The alloy 1163 was produced at the Kamensk-Uralsky Metallurgical Plant and was purchased in the form of 2 mm thick sheets. Samples of 10×10 mm in size for structural studies and 9.0×1.9 mm in size for three-point bending mechanical tests were cut out of them using spark erosion. The composition of the alloy under study was determined by the EDS analysis and is shown in the Table 1. As one can see, the main alloying elements of the 1163 alloy are copper and magnesium. The transition from incomplete to complete GB wetting was observed in binary alloys of aluminum with magnesium [13] and copper [14]. This fact allowed us to count on the observation of the GB wetting phase transition also in the multicomponent 1163 alloy.

Table 1. Composition of the purchased 1163 alloy.

Elements, wt.%								
Al	Mg	Cu	Zn	Mn	Fe	Si	Ti	Ni
91.96	1.50	4.20	0.02	0.58	0.12	0.06	0.06	0.01

The samples were annealed in a SNOL resistance furnace in air at temperatures of 500, 510, 520, 530, 540, 550, 560, 570, 580, 590 and 600°C for 1 hour. The annealing temperature was maintained with an accuracy of ±2°C. After annealing, the samples were quenched in water at room temperature. Scanning electron microscopy (SEM) studies were performed on a Vega TS5130 MM (Tescan) microscope equipped with a LINK energy dispersive spectrometer (EDS, Oxford Instruments). X-ray diffraction analysis (XRD) was performed on a smartLAB diffractometer (Rigaku), $Cu_{K\alpha}$ radiation. The phase analysis and calculation of the crystal lattice parameters were performed using the PowderCell 2.4 program (PowderCell for Windows. Version 2.4. 08.03.2000, Werner Kraus and Gert Nolze, BAM, Berlin). In structural studies, the grain boundary, which contained a layer of the second phase throughout from one GB triple junction to the other, was considered to be completely wetted. When determining the fraction of completely wetted GBs, at least 100 GBs were analyzed. The three-point bending studies were carried out using the TCB 111.2-50 machine (Testsystems LLC, Ivanovo, Russian Federation) at room temperature. During three-point bending tests, 9.0×1.9 mm samples are placed on fixed supports, then a concentrated force load is applied to them in the middle of the distance between the supports (in our case 7.5 mm). An inhomogeneous stress is created in the bent sample. The lower part becomes stretched, and the upper part becomes compressed. In this case, the stresses associated with the bending moment are different in length and cross-section of the sample. During the tests, the software registered the load-deflection (deformation) relationship. Then the deformation curves were used to calculate the Young's modulus, conditional yield strength $\sigma_{0.2}$ and other parameters.

3. Results and discussion

Figure 1 shows SEM micrographs of 1163 alloy samples annealed at temperatures of 500°C (a), 560°C (b) and 600°C (c, d). The grains of the aluminum matrix look dark in the micrographs. The GB interlayers of the melt solidified during quenching and individual particles in the grain bulk look light in the micrographs. The solidified melt in GBs is enriched in copper and magnesium, it and contains mainly the Al_2CuMg phase (see Table 2, composition is determined by EDS in SEM mode and crystallography of phases was determined by XRD). The particles in the grain bulk are enriched in copper, manganese and iron and have the crystallographic structure of Al_2Cu phase (see Table 2). After annealing at 500°C (Fig. 1a) the melt solidified during quenching has the form of individual particles, both in volume and at grain boundaries. Thus, the fraction of completely wetted GBs at 500°C is zero (Fig. 2). At 560°C (Fig. 1b), the sample already contains completely wetted GBs. Here, a continuous layer of liquid phase extends from one GB triple junction to the next one. The fraction of such completely wetted GBs is approximately 30% (Fig. 2). And finally, at a temperature of 600°C (Fig. 1c), almost all GBs in aluminum are completely wetted with melt (Fig. 2). In Fig. 1d the microstructure of a sample annealed at 600°C is shown on an enlarged scale. It is clearly seen that the melt, which wetted GBs during annealing, decomposes into different phases during quenching (see Table 2).

Thus, the fraction of completely wetted GBs in aluminum increases in the studied temperature range from zero to almost 100%. The temperature dependence of the fraction of completely wetted GBs is shown in Fig. 2. Between 500 and 520°C, no completely wetted boundaries between aluminum grains are observed in annealed samples. At the same time, in the sample annealed at a temperature of 530°C, the fraction of completely wetted boundaries are already about 5%. This means that the first fully wetted GBs appear between temperatures between 520 and 530°C around T_{wmin} = 525°C. With a further increase in temperature, the fraction of completely wetted GBs gradually increases to about 80% at 600°C. When the samples were annealed at higher temperatures, there was very little solid phase in them and it was rather difficult to obtain reasonable quantitative

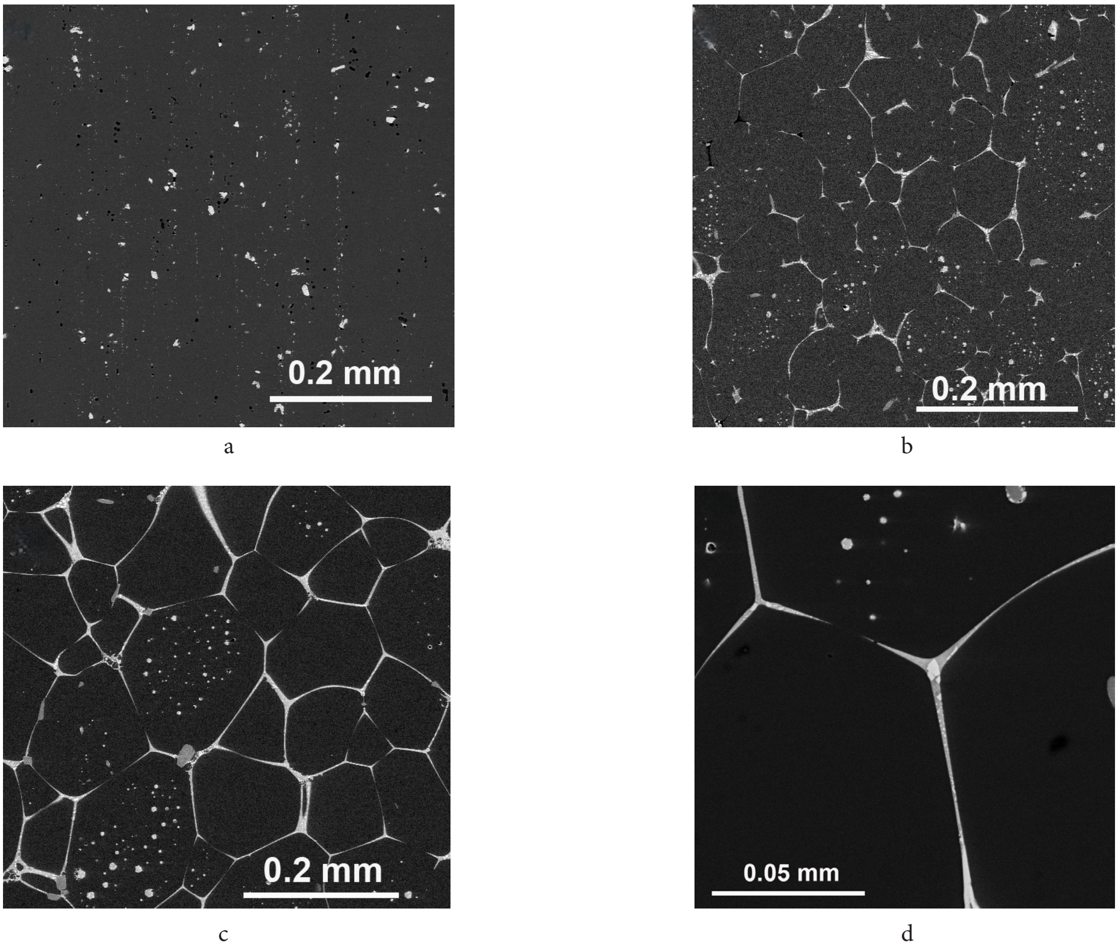

Fig. 1. SEM micrographs of 1163 alloy samples annealed at temperatures of 500°C (a), 560°C (b) and 600°C (c, d).

Table 2. Composition of the structural components of the 1163 alloy pre-annealed at 600°C after quenching. Percentage of phases is estimated by XRD.

Area	Elements, wt.%						Phase	Fraction of phase
	Al	Mg	Cu	Mn	Fe	Si		
Grains	96.5	1.0	1.9	0.6	0.1	0.0	(Al)cub	97 vol.%
Wetting phase	58.4	7.0	32.3	0.6	1.1	0.5	Al_2CuMg	2 vol.%
Inclusions	71.8	0.6	3.3	13.4	10.8	0.2	Al_2Cu	1 vol.%

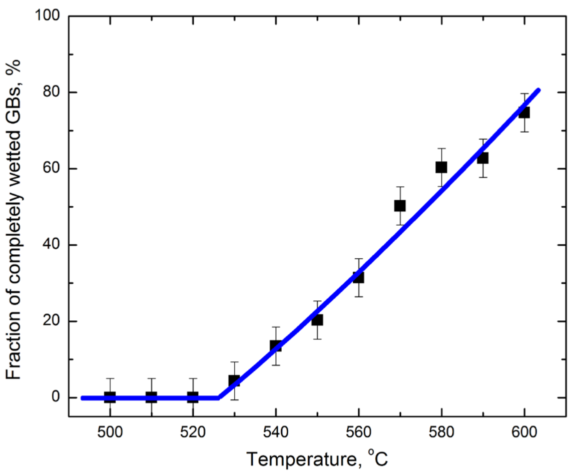

Fig. 2. (Color online) Dependence of the fraction of completely wetted GBs on the annealing temperature in the 1163 alloy. $T_{wmin} = 525$°C.

data on the microstructure. On the other hand, this means that the fraction of completely wetted GBs increases further, above 80% at $T > 600$°C.

Figure 3 shows the stress-vs.-strain deformation curves for samples annealed at temperatures of 520, 530, 550 and 590°C. The figure also contains a scheme for determining the value of the conditional yield strength $\sigma_{0.2}$. The blue dotted line shows that the sample at a temperature of 510°C initially deforms elastically and the stress linearly increases with increasing deformation. The slope of the blue dotted line gives us the value of the Young's modulus. At a stress of about 300 MPa, the strain curve deviates from the linear dependence, this is the elastic limit. The red dotted line parallel to the blue dotted one is drawn 0.2% to the right. Its intersection with the deformation curve gives us the value of the conditional yield strength $\sigma_{0.2}$.

Figures 4 and 5 show, respectively, the dependences of the conditional yield strength $\sigma_{0.2}$ and Young's modulus measured using the quenched samples on the pre-annealing

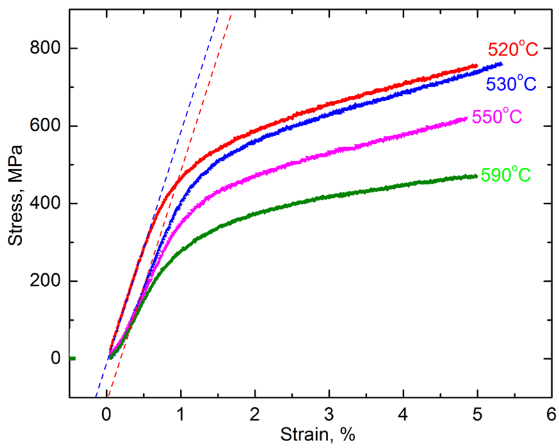

Fig. 3. (Color online) Stress-strain dependences (strain curves) for samples annealed at temperatures 520, 530, 550 and 590°C. A scheme for determining the conditional yield strength $\sigma_{0.2}$ is also given.

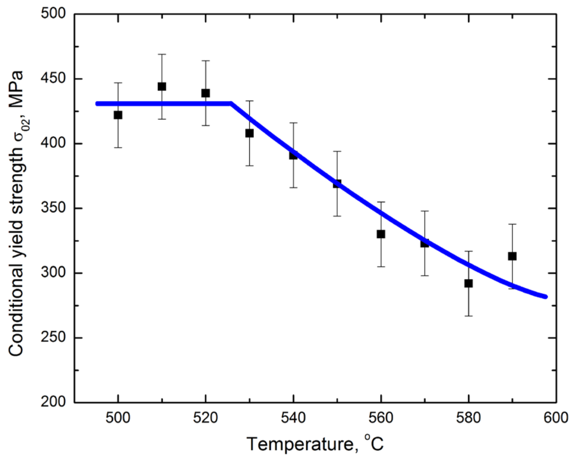

Fig. 4. (Color online) Dependence of the conditional yield strength $\sigma_{0.2}$ on the pre-annealing temperature.

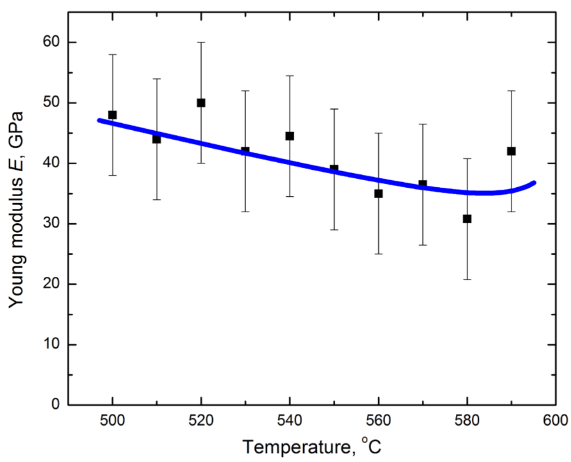

Fig. 5. (Color online) Dependence of the Young's modulus on the pre-annealing temperature.

temperature. In the range from 500 to 520°C, the conditional yield strength $\sigma_{0.2}$ practically does not change with increasing pre-annealing temperature and is about 430 MPa. Then $\sigma_{0.2}$ begins to decrease and gradually drops to a level of about 300 MPa in the sample pre-annealed at a temperature of 590°C. If we compare this dependence with Fig. 2, we will see that in the range from 500 to 520°C, the fraction of completely wetted boundaries is zero. The conditional yield strength $\sigma_{0.2}$ for the quenched samples pre-annealed between 500 to 520°C is also constant. Above 520°C, the fraction of completely wetted GBs begins to increase. This is accompanied by a decrease in the conditional yield strength $\sigma_{0.2}$. Thus, we can conclude that changes in the morphology of the distribution of the liquid phase along GBs and an increase in the fraction of GBs completely covered with Al_2CuMg phase after quenching lead to a decrease in the value of the conditional yield strength $\sigma_{0.2}$. The appearance of continuous layers of the second phase along the boundaries facilitate the deformation of the sample, and it begins to deform plastically at lower applied stresses. To be honest, we have to mention here that the mean grain size increases from about 95 + 5 µm at 560°C to 132 + 5 µm at 600°C. The decreasing grain size can also slightly influence the $\sigma_{0.2}$ value. The Young's modulus almost monotonically decreases from about 50 to 40 GPa with increasing temperature from 500 to 590°C (Fig. 5). We see that the Young's modulus is insensitive to the morphology of the distribution of the second phase along GBs and, apparently, is determined by the elastic properties of the grains themselves, and not by the GBs.

Thus, we found that the transition from incomplete GB wetting to complete one in the 1163 Al-based alloy significantly affects the value of the conditional yield strength $\sigma_{0.2}$. It can be assumed that the GB wetting (and the appearance of a grid of continuous layers of the second phase along the boundaries) leads to a decrease in the barrier for the movement of sliding bands (Chernov–Luders bands) between neighboring grains during plastic deformation. Here, the decrease in the conditional yield strength $\sigma_{0.2}$ can be explained by the fact that with increasing temperature — in accordance with the phase diagram — the aluminum matrix is purified from impurities that pass into the liquid phase. Thus, the total concentration of impurities in the aluminum matrix (measured by EDS in SEM) drops from 6 wt.% at 500°C to 4 wt.% at 600°C. As a result, the grain body is cleansed of impurities and became more plastic. This process will also lead to lower yield strength. These processes occur simultaneously and it is very difficult to give preference to one of them at this stage of research. Thus, the observed effect is very significant and can, both positively and negatively affect the mechanical properties of materials. Therefore, it certainly deserves further more detailed research.

It is worth noting here that signs of GB wetting by melt and the second solid phase are indeed observed in many industrial aluminum alloys during various treatments [15–34]. Grain boundary wetting phenomena have been observed not only in aluminum alloys, but also in steels [9,10,35,36], titanium-based alloys [37–39], tin alloys [1,40], copper alloys [41–44], lithium alloys [45], WC-based cemented carbides [46,47], in magnesium alloys [48,49], Nd-Fe-B based alloys for permanent magnets [50,51], as well as in multicomponent high-entropy alloys [52,53]. This means that the phenomenon that we observe in this work (namely, the relationship between GB wetting and the mechanical properties of the material as a whole) is apparently not limited to the studied 1163 alloy, but has a much more general character and should be observed in a wide range of materials.

Thus, the purpose of this work was not to further improve the properties of the already well-developed and thoroughly studied alloy 1163. Our task was to demonstrate how the appearance of solid layers of the second phase between the matrix grains can strongly change the mechanical properties of the alloy. Alloy 1163, due to the fact that it is well known and studied, seemed to us a good object to demonstrate the difference in the mechanical properties of two different structures: one in which the second solid phase forms continuous layers between the grains of the matrix and the second where the same phase is located along the grain boundaries and has a shape of separate particles. What this effect is, positive or negative, in each case depends on the properties of the second phase at GBs. If the second phase is hard and brittle, then its continuous layer in GB can embrittle the material, such as during the formation of a cementite mesh in hyper-eutectoid steels. If the second phase is ductile and easily to deform, then its presence in GBs can lead, for example, to superplasticity, as is the case in a number of aluminum-based alloys.

Conclusions

1. The paper studies the microstructure evolution in the polycrystalline aluminum alloy 1163, containing copper and magnesium, after a series of annealing between liquidus and solidus in the temperature range from 500 to 600°C.

2. Below 520°C, there is no complete wetting of the Al/Al grain boundaries by the melt. The melt has the shape of spherical droplets in the bulk and lenticular droplets at grain boundaries.

3. Above 520°C, completely wetted grain boundaries appear in the samples, where a melt layer separates one grain of the matrix from another.

4. The wetting layer at the grain boundaries is enriched in copper and magnesium and, after solidification during quenching, contains mainly intermetallic phase Al_2CuMg.

5. The mechanical properties measured using three-point bending significantly depend on the presence of completely wetted GBs (filled with the Al_2CuMg phase)

6. With an increase in the fraction of completely wetted GBs (filled with the Al_2CuMg phase) from 0 to 80%, the conditional yield strength $\sigma_{0.2}$ of the sample rapidly decreases.

7. The Young's modulus, which is mainly determined by the properties of the grain volume, weakly depends on the pre-annealing temperature.

8. Thus, it was shown for the first time that the transition from incomplete GB wetting to complete one can significantly change the mechanical properties of a polycrystal as a whole.

References

1. B. B. Straumal, W. Gust, T. Watanabe, Tie lines of the grain boundary wetting phase transition in the Zn-rich part of the Zn-Sn phase diagram, Mater. Sci. Forum 294/296 (1999) 411–414.
2. S. G. Protasova, O. A. Kogtenkova, B. B. Straumal, P. Zięba, B. Baretzky, Inversed solid-phase grain boundary wetting in the Al-Zn system, J. Mater. Sci. 46 (2011) 4349–4353.
3. B. Straumal, E. Rabkin, W. Lojkowski, W. Gust, L.S. Shvindlerman, Pressure influence on the grain boundary wetting phase transition in Fe-Si alloys, Acta mater. 45, 5 (1997) 1931–1940.
4. B. Straumal, N. E. Sluchanko, W. Gust, Influence of the grain boundary phase transitions on the properties of Cu-Bi polycrystals, Def. Diff. Forum 188–190 (2001) 185–194.
5. B.B. Straumal, A.A. Mazilkin, S.G. Protasova, A.A. Myatiev, P.B. Straumal, E. Goering, B. Baretzky, Influence of texture on the ferromagnetic properties of nanograined ZnO films, Phys. Stat. Sol. B 248 (2011) 581–586.
6. B.B. Straumal, A.A. Myatiev, P.B. Straumal, A.A. Mazilkin, S.G. Protasova, E. Goering, B. Baretzky, Grain boundary layers in nanocrystalline ferromagnetic zinc oxide, JETP Letters 92 (2010) 396–400.
7. B.B. Straumal, A.A. Mazilkin, S.G. Protasova, P.B. Straumal, A.A. Myatiev, G. Schütz, E. Goering, B. Baretzky, Ferromagnetism of nanostructured zinc oxide films, Phys. Metal. Metallogr. 113 (2012) 1244–1256.
8. S.G. Protasova, B.B. Straumal, A.A. Mazilkin, S.V. Stakhanova, P.B. Straumal, B. Baretzky, Increase of Fe solubility in ZnO induced by the grain boundary adsorption, J. Mater. Sci. 49 (2014) 4490–4498.
9. O.I. Noskovich, E.I. Rabkin, V.N. Semenov, B.B. Straumal, L.S. Shvindlerman, Wetting and premelting phase transitions in 38° [100] tilt grain boundaries in (Fe-12 at.%Si)-Zn alloy in the vicinity of the A_2-B_2 bulk ordering in Fe-12at.%Si alloy, Acta metall. mater. 39 (1991) 3091–3098.
10. B.B. Straumal, O.I. Noskovich, V.N. Semenov, L.S. Shvindlerman, W. Gust, B. Predel, Premelting transition on 38°<100> tilt grain boundaries in (Fe-10 at.%Si)-Zn alloys, Acta metall. mater. 40 (1992) 795–801.
11. S.V. Divinski, M. Lohmann, Chr. Herzig, B. Straumal, B. Baretzky, W. Gust, Grain boundary melting phase transition in the Cu-Bi system, Phys. Rev. B 71 (2005) 104104.
12. B. Bian, S. Taheriniya, G. Mohan Muralikrishna, A. Godha, S.K. Makineni, S. Sankaran, B.B. Straumal, Y. Du, G. Wilde, S.V. Divinski, Kinetic and structural insights into the grain boundary phase transitions in Ni-Bi alloys, Acta Mater. 245 (2022) 118632.
13. O.A. Kogtenkova, S.G. Protasova, A.A. Mazilkin, B.B. Straumal, P. Zięba, T. Czeppe, B. Baretzky, Heat effect of grain boundary wetting in Al-Mg alloys. J. Mater. Sci. 47 (2012) 8367–8371.
14. B. B. Straumal, O. A. Kogtenkova, A. N. Nekrasov, J. Dutta Majumdar, G. Faraji, D. Bradai, Grain boundary wetting phenomena in the Al-Cu system. Lett. Mater. 14 (2024) 319–324.
15. P. Zhao, Z. Li, Z. Xu, X. Leng, A. Tong, J. Yan, Migrating behaviors of interfacial elements and oxide layers during diffusion bonding of 6063Al alloys using Zn interlayer in air, J. Mater. Sci. Technol. 155 (2023) 119–131.

16. A. Mochugovskiy, N. Tabachkova, A. Mikhaylovskaya, Annealing induced precipitation of nanoscale icosahedral quasicrystals in aluminum based alloy, Mater. Lett. 247 (2019) 200 – 203.
17. B. B. Straumal, O. A. Kogtenkova, M. Yu. Murashkin, M. F. Bulatov, T. Czeppe, P. Zięba, Grain boundary wetting transition in Al-Mg alloys. Mater. Lett. 186 (2017) 82 – 85.
18. N. Q. Chinh, P. Jenei, J. Gubicza, E. V. Bobruk, R. Z. Valiev, T. G. Langdon, Influence of Zn content on the microstructure and mechanical performance of ultrafine-grained Al-Zn alloys processed by high-pressure torsion, Mater. Lett. 186 (2017) 334 – 337.
19. A. Q. Ahmed, D. Ugi, J. Lendvai, M. Yu. Murashkin, E. V. Bobruk, R. Z. Valiev, N. Q. Chinh, Effect of Zn content on microstructure evolution in Al-Zn alloys processed by high-pressure torsion, J. Mater. Res. 38 (2023) 3602.
20. M. Xu, Z. Zheng, D. Han, R. Ma, A. Du, Y. Fan, X. Zhao, X. Cao, Wetting of liquid zinc-aluminum-magnesium alloy on steel substrate during hot-dipping: Understanding the role of the flux, Surf. Topogr.: Metrol. Prop. 10 (2022) 035038.
21. Y. R. Chen, Examination and analysis of 2 Pct Mg-55 Pct Al-1.6 Pct Si-Zn coating on steel, Metal. Mater. Trans. A 51 (2020) 5758 – 5770.
22. N. Q. Chinh, P. Szommer, J. Gubicza, M. El-Tahawy, E. V. Bobruk, M. Yu. Murashkin, R. Z. Valiev, Characterizing microstructural and mechanical properties of Al-Zn alloys processed by high-pressure torsion, Adv. Eng. Mater. 22 (2020) 1900672.
23. J. L. C. Quintana, S. S. Medina, M. Hernández, O. M. Suárez, Study of thermomechanical properties of an Al-Zn-based composite reinforced with dodecaboride particles, Adv. Mater. Sci. Eng. 2018 (2018) 2975234.
24. A. Baris, N. Q. Chinh, R. Z. Valiev, T. G. Langdon, Microstructure decomposition and unique mechanical properties in an ultrafine-grained Al-Zn alloy processed by high-pressure torsion, Kovove Mater. 53 (2015) 251 – 258.
25. B. B. Straumal, A. A. Mazilkin, X. Sauvage, R. Z. Valiev, A. B. Straumal, A. M. Gusak, Pseudopartial wetting of grain boundaries in severely deformed Al-Zn alloys, Russ. J. Non-Ferr. Met. 56 (2015) 44 – 51.
26. Y. Yuan, X. Liu, G. Pu, T. Wang, Q. Guo, Corrosion features and time-dependent corrosion model of Galfan coating of high strength steel wires, Constr. Build. Mater. 313 (2021) 125534.
27. N. Kalantarrashidi, M. Alizadeh, S. Pashangeh, Microstructure evolution and mechanical properties evolution of high-Zn Al-Zn alloys prepared by cross accumulative roll bonding combined with heat treatment process, J. Alloys Compd. 927 (2022) 167042.
28. T. Liu, R. Ma, Y. Fan, A. Du, X. Zhao, M. Wen, X. Cao, Effect of fluxes on wettability between the molten Galfan alloy and Q235 steel matrix, Surf. Coat. Technol. 337 (2018) 270 – 278.
29. X. Zhang, C. Leygraf, I. Odnevall Wallinder, Selected area visualization by FIB-milling for corrosion-microstructure analysis with submicron resolution, Mater. Lett. 98 (2013) 230 – 233.
30. X. Zhang, C. Leygraf, I. Odnevall Wallinder, Atmospheric corrosion of Galfan coatings on steel in chloride-rich environments, Corr. Sci. 73 (2013) 62 – 71.
31. X. Zhou, W. Shi, S. Xiang, Improving corrosion resistance of Zn-5wt.% Al alloy by microalloying with samarium, J. Rare Earths 41 (2023) 1636 –1644.
32. T. Gancarz, J. Pstrus, G. Cempura, K. Berent, Influence of Li addition to Zn-Al alloys on Cu substrate during spreading test and after aging treatment, J. Electron. Mater. 45 (2016) 6067 – 6078.
33. T. Gao, L. Liu, S. Liu, C. Yuan, Y. Bian, X. Liu, The growth behavior of Al_2Cu phase in confined spaces constituted by γ-Al_2O_3 particle clusters, Mater. Lett. 304 (2021) 130711.
34. T. Gao, Y. Bian, L. Liu, K. Zhao, K. Hu, X. Liu, Modification of primary and eutectic phases in Al-33.2Cu and Al-20Mg_2Si alloys by nano-treating, Mater. Lett. 286 (2021) 129218.
35. M. Günen, A. Bakkaloğlu, Influence of sinter-hardening on microstructures and mechanical properties of Astaloy Mo-based steels, Mater. Lett. 251 (2019) 201 – 205.
36. M. I. Abdulsalam, Study of simulated disbonded polymer film on Zn-Al alloy coated reinforcing steel rebars, Corr. Sci. 138 (2018) 307 – 318.
37. S. Shukla, V. Bajpai, Effect of cryogenic quenching on microstructure and microhardness of Ti-6Al-4V alloy. Mater. Lett. 267 (2020) 127532.
38. X. Huang, Y. Feng, J. Ge, X. Meng, Y. Wang, L. Li, Z. Li, M. Ding, Electron irradiation mechanism of Ti_3AlC_2 material by in situ observation, Mater. Lett. 262 (2020) 127061.
39. A. S. Gornakova, S. I. Prokofiev, B. B. Straumal, K. I. Kolesnikova, Growth of (αTi) grain boundary layers in Ti-Co alloys, Russ. J. Non-Ferr. Met. 57 (2016) 703 – 709.
40. W. C. Ting, H. Yong, T. G. Langdon, The significance of strain weakening and self-annealing in a superplastic Bi-Sn eutectic alloy processed by high-pressure torsion, Acta Mater. 185 (2020) 245 – 256.
41. S. Gorsse, B. Ouvrard, M. Gouné, A. Poulon-Quintin, Microstructural design of new high conductivity – high strength Cu-based alloy, J. Alloys Compd. 633 (2015) 42 – 47.
42. S. Shu, X. Zhang, P. Bellon, R. S. Averback, Non-equilibrium grain boundary wetting in Cu-Ag alloys containing W nanoparticles, Mater. Res. Lett. 4 (2016) 22 – 26.
43. L.-S. Chang, B. B. Straumal, E. Rabkin, W. Gust, F. Sommer, The solidus line of the Cu-Bi phase diagram, J. Phase Equil. 18 (1997) 128 –135.
44. B. B. Straumal, O. A. Kogtenkova, A. B. Straumal, B. Baretzky, Grain boundary wetting-related phase transformations in Al and Cu-based alloys, Lett. Mater. 8 (2018) 364 – 371.
45. G. Wang, D. Song, C. Li, E. E. Klu, Y. Qiao, J. Sun, J. Jiang, A. Ma, Developing improved mechanical property and corrosion resistance of Mg-9Li alloy via solid-solution treatment, Metals 9 (2019) 920.
46. B. B. Straumal, I. Konyashin, B. Ries, A. B. Straumal, A. A. Mazilkin, K. I. Kolesnikova, A. M. Gusak, B. Baretzky, Pseudopartial wetting of WC/WC grain boundaries in cemented carbides, Mater. Lett. 147 (2015) 105 –108.

47. A. A. Mazilkin, B. B. Straumal, S. G. Protasova, M. F. Bulatov, B. Baretzky, Pseudopartial wetting of W/W grain boundaries by the nickel-rich layers, Mater. Lett. 192 (2017) 101–103.
48. B. Straumal, K. Tsoy, A. Druzhinin, V. Orlov, N. Khrapova, G. Davdian, G. Gerstein, A. Straumal, Coexistence of intermetallic complexions and bulk particles in grain boundaries in the ZEK100 alloy, Metals 13 (2023) 1407.
49. B. Straumal, N. Khrapova, A. Druzhinin, K. Tsoy, G. Davdian, V. Orlov, G. Gerstein, A. Straumal, Grain boundary wetting transition in the Mg-based ZEK 100 alloy, Crystals 13 (2023) 1538.
50. A. Mazilkin, B. B. Straumal, S. G. Protasova, S. Gorji, A. B. Straumal, M. Katter, G. Schütz, B. Baretzky, Grain boundary oxide layers in NdFeB-based permanent magnets, Mater. Design 199 (2021) 109417.
51. B. B. Straumal, Yu. O. Kucheev, I. L. Yatskovskaya, I. V. Mogilnikova, G. Schütz, B. Baretzky, Grain boundary wetting in the NdFeB-based hard magnetic alloys, J. Mater. Sci. 47 (2012) 8352–8359.
52. X. Gao, Y. Lu, Laser 3D printing of CoCrFeMnNi high-entropy alloy, Mater. Lett. 236 (2019) 77–80.
53. P. Sreeramagiri, G. Balasubramanian, Directed energy deposition of multi-principal element alloys, Front. Mater. 9 (2022) 825276.